frontiers | Frontiers in Earth Science

TYPE Original Research
PUBLISHED 22 October 2024
DOI 10.3389/feart.2024.1407902

OPEN ACCESS

EDITED BY
Gang Rao,
Southwest Petroleum University, China

REVIEWED BY
Renqi Lu,
China Earthquake Administration, China
Yiquan Li,
Nanjing University, China

*CORRESPONDENCE
Liang Qiu,
qiul@cugb.edu.cn

RECEIVED 27 March 2024
ACCEPTED 12 July 2024
PUBLISHED 22 October 2024

CITATION
Xu H, Qiu L, Yan D-P and Wang X-W (2024) Geometry of large normal fault growth and linkage with temporal constraints: a case study on the Lanliao fault in Dongpu Sag, Bohai Bay basin, NE China.
Front. Earth Sci. 12:1407902.
doi: 10.3389/feart.2024.1407902

Geometry of large normal fault growth and linkage with temporal constraints: a case study on the Lanliao fault in Dongpu Sag, Bohai Bay basin, NE China

Han Xu[1,2,3], Liang Qiu[3]*, Dan-Ping Yan[3] and Xin-Wen Wang[3]

[1]General Prospecting Institute of China National Administration of Coal Geology, Beijing, China, [2]Key Laboratory of Transparent Mine Geology and Digital Twin Technology, National Mine Safety Administration, Beijing, China, [3]State Key Laboratory of Geological Processes and Mineral Resources, School of Earth Sciences and Resources, China University of Geosciences, Beijing, China

The Dongpu Sag exhibits highly representative structural features of the Bohai Bay Basin. By utilizing time depth quantification (TDQ) technology, geological profiles were generated through the processing of seismic data with a velocity model. These profiles were integrated to investigate the linkage geometry and timing of the Lanliao fault, the eastern boundary fault of the Dongpu Sag. Structural analysis revealed at least five original fault segments of the Lanliao fault, each initiating independently during the early growth phase. The development of these isolated fault segments began in the early Eocene, which is concurrent with the deposition of the Es_4 member. The southern fault segments were active earlier but became inactive later as the northern segments gained activity during the Es_3 member. Transverse anticlines separate the northern and southern faults. By the time of the Es_2 member, all segments had linked, forming a continuous boundary fault across the transverse anticlines. As the Dongpu Sag expanded, the depocenter relocated. The southern fault formed a graben, known as the Gegangji subsag, controlling the depocenter during the Es_3^3 and Es_3^2 members. The depocenter of the Es_3^1 member shifted northward swiftly, developing into a half-graben depocenter called the Huzhuangji subsag. In the post-linkage development phase, the activity of the Lanliao fault decreased over time, with displacement becoming more concentrated on the Huanghe fault, an intrabasin fault. The Huanghe fault then dominated basin sedimentation, moving the depocenter to the Mengmangji subsag. This study demonstrates that the fault linkage is a significant event in basin evolution, exerting considerable control over sedimentation and the overall evolution of the basin.

KEYWORDS

Bohai Bay Basin, Dongpu Sag, Lanliao fault, linkage timing and geometry, linkage pattern

1 Introduction

Large normal faults in rifting basins are typically composed of overstepping or linked segments along their strike over a wide range of scales (Gawthorpe and Leeder, 2000; Peacock, 2002). Over the last few decades, significant attention has been given to investigating the temporal evolution of large normal faults using seismic data. Research on fault development has commonly suggested that large faults are often formed through the linkage of smaller fault segments (Morley, 1999; Soliva and Benedicto, 2004; Higgins et al., 2007; Su et al., 2011; Wang et al., 2018; Phoosongsee and Morley, 2019). These studies have focused on understanding the mechanics of interaction and the linkage processes between fault segments, as well as gaining insights into fault displacement variations along strike and dip, fault development, and fault linkage geometry. Fault linkage geometry can follow three possible paths: 1) small faults develop independently and control the depocenter occupying the major syn-rift period, and boundary fault linkage occurs at a later syn-rift stage and controls minor basin filling. 2) Rapid fault linkage during the early syn-rift stage forms a boundary fault prior to significant basin development; once linked, the boundary fault maintains its strike length, and deposition is confined. (3) A range of geometries between (1) and (2), where fault growth and linkage occur during basin development, accompanied by simultaneous material filling and deposition (Ebinger et al., 1989; Schlische, 1991; Schlische and Anders, 1996; Morley, 1999; Morley, 2002; Fontijn et al., 2010; Su et al., 2011; Macgregor, 2014; Liu et al., 2017; Lucas et al., 2023). Coupling structural geology with deposition allows the observation of when, where, and how major normal faults reshape the stratigraphic architecture of the basin. The completion of the boundary fault linkage does not mark the end of basin development during the syn-rift stage (Morley, 1999; Mcleod et al., 2000; Morley, 2002; Su et al., 2011; Fossen and Rotevatn, 2016; Wang et al., 2018; Li J. et al., 2021a; Lucas et al., 2023). The post-linkage evolution of intra-basin faults is crucial in the evolutionary history of rifting basins. To examine the details of when, where, and how a major basin-bounding fault developed throughout the entire syn-rift stage, the Lanliao Fault of the Dongpu Sag was investigated.

The Dongpu Sag, located in the southwestern Bohai Bay Basin, was selected for this study due to its high exploration level and abundant seismic data sets. This sag exhibits a high density of

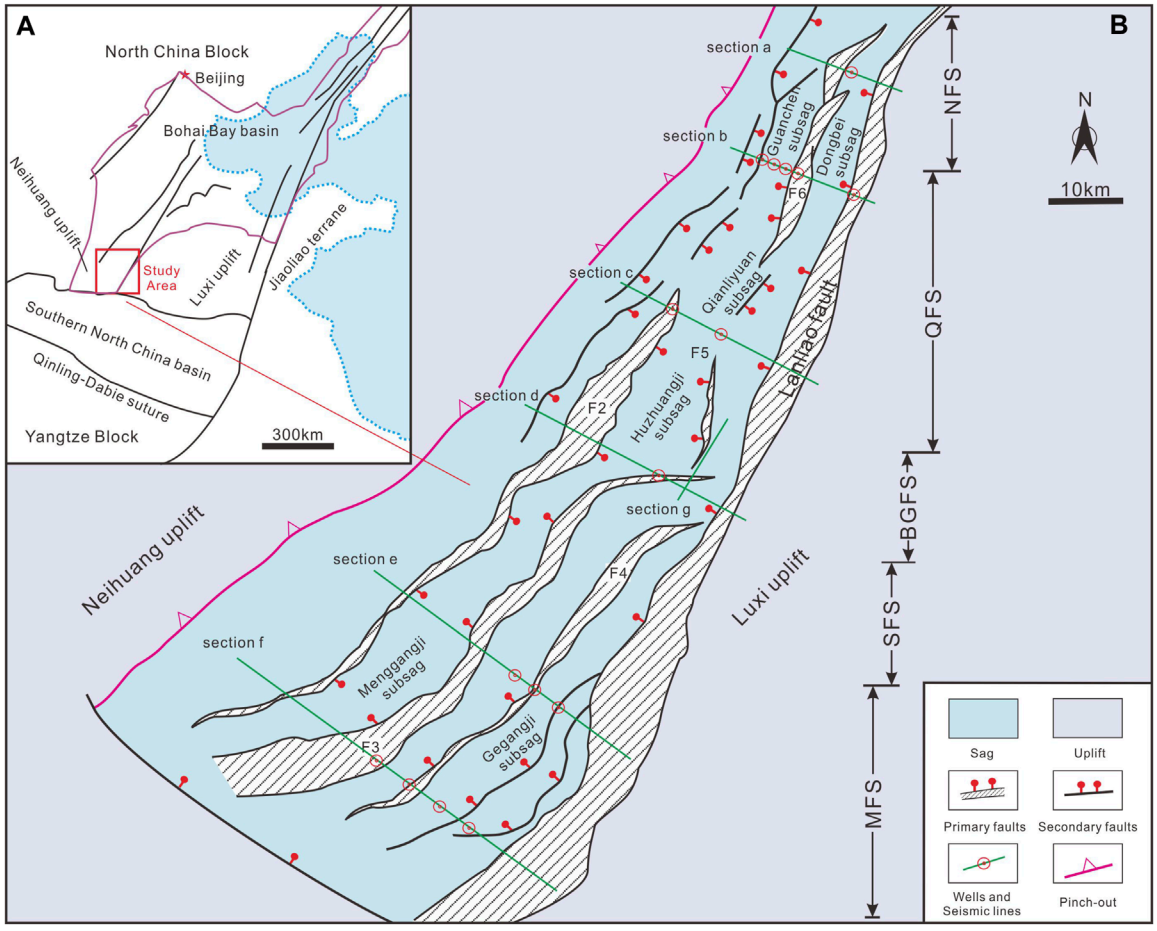

FIGURE 1
(A) Regional location of the Dongpu Sag within the Bohai Bay Basin (modified after Huang et al., 2014), and **(B)** tectonic settings of the Dongpu Sag, major fault morphology (e.g., the Lanliao fault, F2: Changyuan fault, F3: Huanghe fault, F4: Machang fault, F5: Duzhai fault, F6: Pucheng fault, F7: Shijiaji fault, and F8: Wendong fault), extracted from the structural sketch of reflection layer H_3 (Xu et al., 2018).

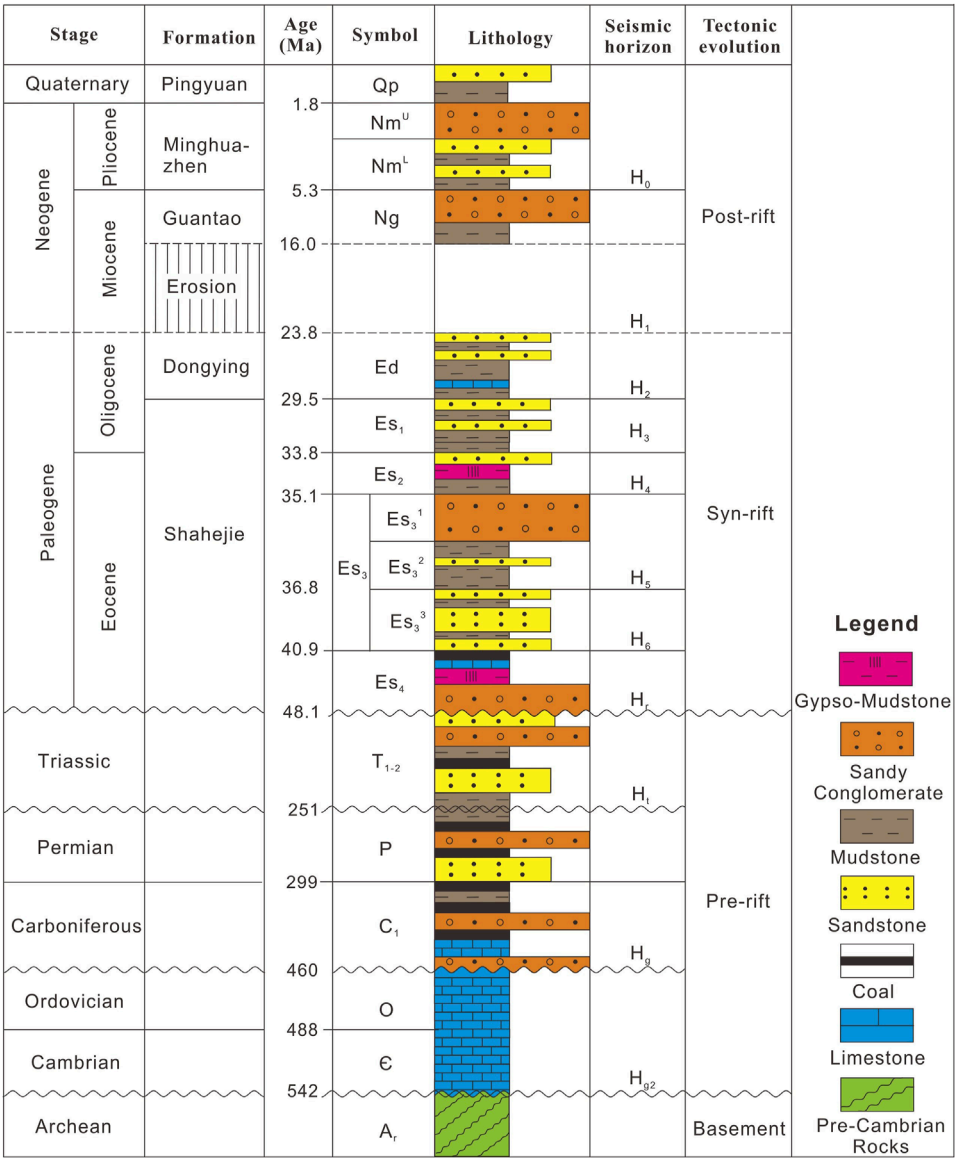

FIGURE 2
Generalized stratigraphic column of the Dongpu Sag (modified after Xu et al., 2018).

normal fault development associated with a back-arc spreading setting during the Cenozoic, as discussed by numerous researchers (e.g., Allen et al., 1997; Ren et al., 2002; Su et al., 2009; Liang et al., 2016). The Lanliao Fault lies in the eastern boundary of the sag, which extends over 170 km from the north to the south. Due to its polycyclic syn-rift development, the Lanliao boundary fault has recorded a significant tectonic and sedimentary history regarding fault growth and linkage (Li J. et al., 2021a). In this study, we combined 2-D and 3-D seismic data to investigate the fault displacement characteristics and the distribution of transfer zones, aiming to identify the original fault segments and their linkage timing and pattern. We also examined the relationship between the fault linkage process and the relocation of the depocenter. In particular, we discussed the post-linkage evolution of the Lanliao Fault, other major intra-basin faults, and the corresponding depocenter relocation.

2 Geological setting

The Dongpu sag is located in the southern part of the Bohai Bay Basin in northeastern China (Figure 1A). It is adjacent to the Luxi Uplift to the east and the Neihuang Uplift to the west, and it is bounded to the south by the southern North China basin (Lu and Qi, 1997; Qi et al., 2006; Xu et al., 2018). The sag comprises six subordinate subsags, namely, Guancheng, Dongbei, Huzhuangji, Qianliyuan, Menggangji, and Gegangji subsags, arranged from northwest to southeast (Figure 1B).

TABLE 1 Average seismic velocity of layers extracted from wells by sonic logging.

Depth/m	Logging depth/m	Time/ms
1,530.5	1,562.53	1,422
1,735.74	1,767.8	1,538
1,836.23	1,868.3	1,608
2,031.64	2,063.72	1,732
2,236.44	2,268.53	1,856
2,431.08	2,463.17	1,972
2,633.85	2,665.94	2,086
2,838.42	2,870.51	2,196
3,038.49	3,071.93	2,296
3,330.78	3,374.71	2,442
3,532.49	3,584.76	2,536
3,738.97	3,800.63	2,634
3,934.8	4,006.57	2,724
4,134.47	4,214.44	2,816
4,336.18	4,423.81	2,912
4,533.06	4,627.2	3,000
4,732.75	4,833.73	3,092
4,932.99	5,043.4	3,184
5,135.01	5,260.28	3,276
5,337.3	5,472.74	3,364
5,538.36	5,680.32	3,448
5,768.88	5,912.73	3,537

The Dongpu Sag formed during the Cenozoic on the Archean and early Paleozoic basement of the North China block (Ren et al., 2002; He and Wang, 2003; Xu et al., 2009; Li et al., 2023). Throughout the Cenozoic, the Dongpu Sag experienced significant extensional faulting and the Dongying tectonic event, which was followed by widespread thermal subsidence (He and Wang, 2003; Qi and Yang, 2010; Hou and Hari, 2014). The typical continental rifting is proposed to be a back-arc extension caused by the eastward subduction of the Pacific plate (Ren, 1996; Wang, 1997; Chen et al., 1998; Zhang et al., 2004; Yin, 2010; Huang et al., 2014; Li T. et al., 2021b). The Dongying tectonic event represents a structural inversion that separated the Paleogene syn-rift sequence from the Neogene post-rift sequence (Zhai, 1993; Hou and Hari, 2014; Yu and Koyi, 2016). Post-rift thermal subsidence led to the extensive deposition of Neogene to Quaternary sediments (Qi, 2004; Huang et al., 2014).

The stratigraphy of the Dongpu Sag is summarized in Figure 2. It consists of, from the bottom to top, Precambrian crystalline basement, Paleozoic marine carbonates and terrestrial clastics, Mesozoic coarse terrestrial clastics and volcanic rocks, and Cenozoic continental clastics and interbedded limestone (Li et al., 2005; Su et al., 2009; Xu et al., 2018). The Paleogene sedimentary sequences comprise the Shahejie (Es) and Dongying (Ed) formations (Yang et al., 2006; Qi and Yang, 2010).

The Shahejie Formation could be divided into four members, i.e., Es_4, Es_3, Es_2, and Es_1 (Qi, 2004; Huang et al., 2014). Generally, Es_4 member deposits are mainly lacustrine and composed of thin sandstone interlayered with mudstone deposits characterized by a coarsening upward reverse cycle sequence (Qi, 2004; Yang et al., 2006). The thick Es_3 member could be divided into sub-members such as Es_3^3, Es_3^2, and Es_3^1 from bottom to top based on fossil and rock assemblages (Li et al., 2005; Qi and Yang, 2010; Xu et al., 2018). Es_3^3 deposited gray mudstone and siltstone interlayered with carbonate. In Es_3^2 deposition, intense rifting and humid paleoclimate expanded the lake basin, resulting in the emergence of deep lake and turbidite facies (Chen et al., 2007; Zeng et al., 2013). During Es_3^1, rifting gradually weakened (Wang et al., 2005; Wang et al., 2011). Es_2 and Es_1 members shared a similar sedimentary environment, depositing gray sandstone interlayered with red mudstone, and salt rock interbed (Chen et al., 2007; Zeng et al., 2013; Ji et al., 2018). The Dongying Formation (Ed) deposited in a broad fluvial–deltaic environment deposits the coarsening upward sequence of clastic rocks (Li et al., 2005; Wang et al., 2011; Shao et al., 2018). Based on seismic stratigraphy, we distinguish eight continuous and traceable stratigraphic seismic horizons (H_r–H_0) in the Cenozoic, representing the base of Es_4, Es_3^3, Es_3^2, Es_2, Es_1, Ed, Ng, and Nm, respectively.

3 Structures of the Dongpu Sag

Seven rare seismic profiles in the time domain are processed into the depth domain by TDQ technology and dozens of wells data. Based on the depth and time relationship of wells, we calculate the average velocity field of the well point (Table 1). The depth-exceeded wells were simulated using Landmark software. Under the constraints of seismic structures, a spatial velocity field of seismic profile is established through interpolation and extrapolation.

3.1 Geometry of faults

The Lanliao Fault is the eastern boundary of the Dongpu Sag. To the east of the fault's footwall lies the Luxi Uplift, while the hanging wall consists of syn-rift Mesozoic–Cenozoic sediments (Qi et al., 2006). The Lanliao fault has a winding shape in plain view with three major strikes (Figure 1). From north to south, these strikes are near NNE, NE, and NS, respectively. Seismic profiles and balanced cross-sections are used to investigate the overall characteristics of faults in the Dongpu Sag (Figures 3–10). These dip cross sections provide geometry controls of the Lanliao Fault, indicating the maximum fault throw approximately 6 km or more.

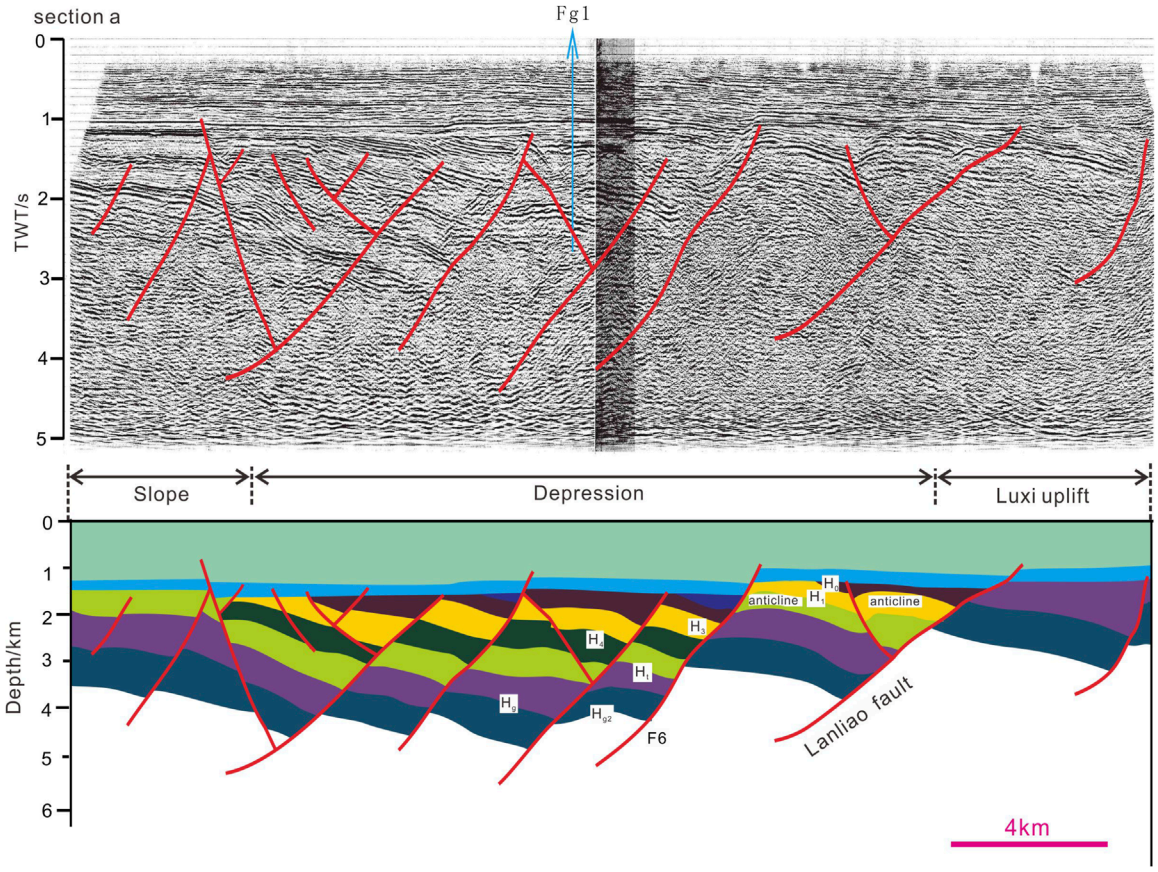

FIGURE 3
Seismic section a (upper) and interpreted (lower) geological profiles crosscut the northern Lanliao fault (Figure 1 for location). TWT, two-way travel time.

The Changyuan fault (fault F2) is a major intra-basin fault in the study zone over 110 km long (Figure 1). F2 locates in the middle–southern sag. It serves as the western boundary controlling syn-rift sedimentary sequences (H_6–H_1). The strike orientation of F2 is roughly parallel to the Lanliao fault, and the fault dips SE. Maximal vertical displacement of F2 is over 6 km, which partially excesses the Lanliao fault. The Huanghe Fault (fault F3) is also important. Unlike F2, fault F3 only controlled the Oligocene sedimentary sequence (H_3–H_1). The strike of F3 is similar to the Lanliao Fault. F2 and F3 together form a graben structure, controlling the Menggangji subsag. F4 and Lanliao Fault in the southern sag suggested a two-stage fault development; the younger F4 (Machang Fault) cross-cut the older Lanliao Fault (Figure 9). Balanced restoration of the Dongpu Sag also suggested two stages of fault development (Liu et al., 2004; Liu, 2009).

In addition to these large-scale faults, a series of secondary faults are developed throughout the sag. These faults are widely distributed in the northern sag (Figure 1). Sparse seismic reflection data demonstrate that these secondary faults have minor displacement (<1,400 m) and control much of the basin geometry (Figures 3–5). Striking obliquely or diagonally to the Lanliao fault, these faults developed during the Late Eocene to the Early Oligocene, relatively late in the basin's evolution (Qi and Yang, 2010). The localization of faults in the southern sag is significant; only two faults developed with large fault displacement over 1,200 m, intersecting the Lanliao Fault obliquely.

Rifting in the central sag concentrates along several secondary faults (e.g., fault F4 and F5). These faults have larger displacements and lengths compared to their northern counterparts, with displacements of up to 1,200 m. Faults F4 and F5 generated vertically near the central boundary fault, extending southwest (F4) and northwest (F5) into the hanging-wall basin, respectively (Figures 7, 8). The sediment characteristics of F5 in both the hanging wall and footwall indicate that F5 is originally formed during the Mesozoic. F5 was reactivated intensively in the Cenozoic along the original fault plane, crosscutting the Paleogene sedimentary sequences (H_1–H_6) toward the northwest.

3.2 Deformation of faults

The kinematics of the Lanliao Fault is reflected in the deformation and sedimentary records of the hanging wall and footwall. The Paleogene sediment in the hanging wall generally dip toward the Lanliao Fault plane, reflecting the characteristics of related fold deformation constrained by normal fault morphology. Due to significant differences in the fault plane morphology along its strike, the deformation of the overlying strata also

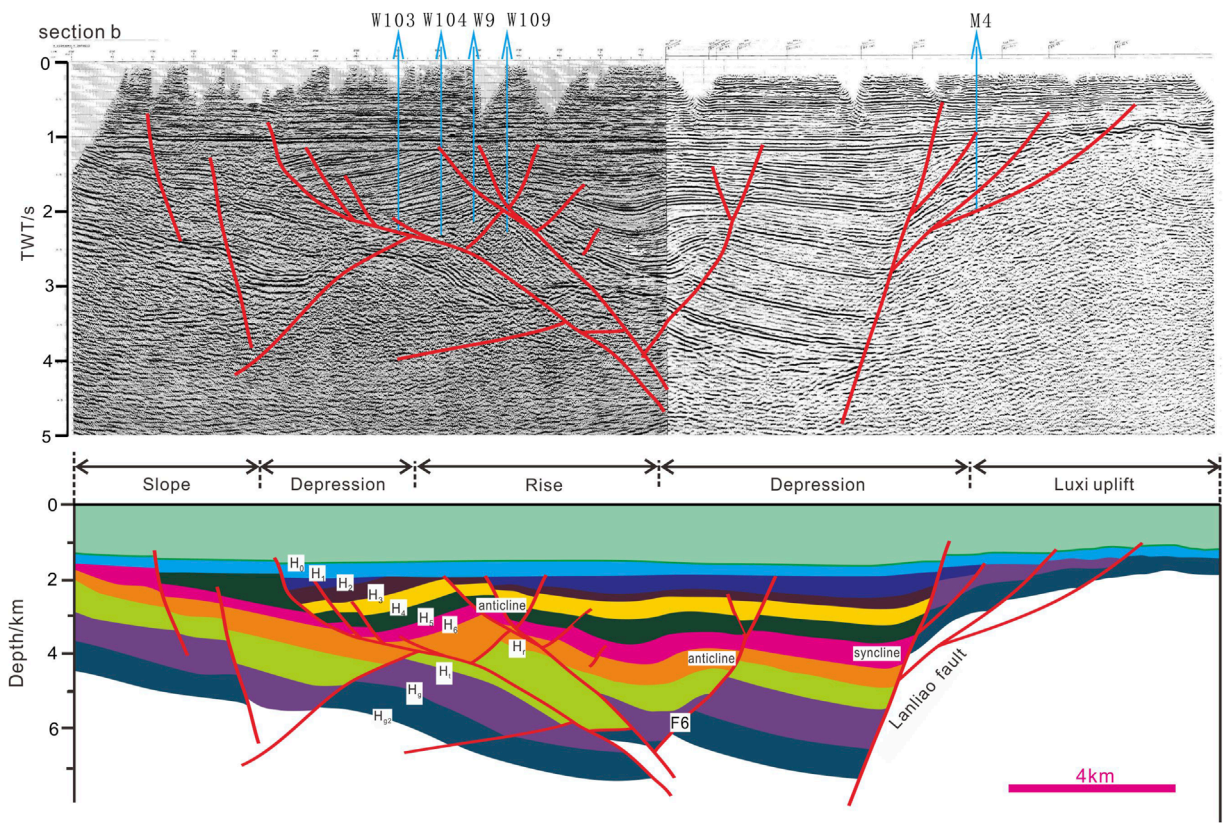

FIGURE 4
Seismic section b (upper) and interpreted (lower) geological profiles crosscut the northern Lanliao Fault (Figure 1 for location). TWT, two-way travel time.

shows variability. The hanging wall deformation is particularly complex within the study zone. The dominant deformation style is characterized by normal fault activities, which are investigated in detail (Allen et al., 1997; Yang et al., 2006; Cheng, 2009; Cheng et al., 2010; Zuo et al., 2017; Xu et al., 2018). Contemporaneous and subsequent folding in the hanging wall is also noteworthy and warrants further attention.

In cross sections, syn-rift sequences (H_r–H_1) in the northern sag exhibit broad wedge-shaped geometry and form a typical half graben. In the southern sag, syn-rift sequences are divided by the intra-basin rise, resulting in a graben–horst–graben pattern. The hanging wall strata thicken toward the boundary fault but thin and onlap onto the dip slope toward the west. Syn-rift strata close to the fault zone generally share similar dip angles with the boundary fault, defining the axis of an asymmetric syncline (Liu et a., 2001). The western limb of the syncline extends into the hanging wall, with the hinge zone forming in associated with the nearby depocenter. The syncline involves different syn-rift strata in various seismic profiles. In Figures 3, 4, sequences H_6–H_1 are all part of the syncline limb, whereas the Dongying Formation (H_2–H_1) is not involved in the syncline, as shown in Figures 6, 7. The syncline near the fault zone is unnoticeable, as shown in Figures 3, 8. The axial trace of the hanging wall asymmetric syncline is parallel to the strike of the Lanliao Fault.

Next to the asymmetric syncline is a W-trending intra-basin high (Figures 6–8). The intra-basin high exhibited neutral fold geometry with symmetric limbs and axial traces perpendicular to the Lanliao Fault. Previous studies have defined this intra-basin high as the transverse anticline, a type of synthetic transfer zone (Liu et al., 2004). Transverse anticline developed parallel to and in the hanging wall of the strike of faults. Fault displacement remained minimal on the anticline axis and increases rapidly toward both fold limbs along the strike into the nearby depocenters (Chen et al., 1998; Liu et al., 2004; Sun, 2007; Sun et al., 2006). Those anticlines are termed 'fault nose' structure or 'buried hill' by Chinese petroleum geologists; and the 'nose' or 'hill' commonly indicates the linkage site of individual fault segments (Su et al., 2011).

Two other types of anticlines are identified in the cross sections. One type abuts the top of the hanging wall with an axial trace parallel to the Lanliao Fault. The anticline consists of Es_2 and Es_1 sediments. Tectonic stress reversal caused the hanging wall of the fault to move upward, forming a series of reverse anticlines (Figure 3). The reverse anticline is related to the widespread Dongying tectonic event that separated the Paleogene and Neogene period in the Bohai Bay Basin (Su et al., 2010; Liang et al., 2016; Xu et al., 2018). The hinge zone is commonly truncated by the H_1 unconformity, denuding Ed and partial Es_1 layers of the anticline. Reverse anticline are commonly observed in the northern sag, indicating intense tectonic movement in the northern sag (Shi et al., 1999).

In addition to reverse anticlines, a set of broad anticlines are recognized in the cross sections. The eastern limb of these anticlines

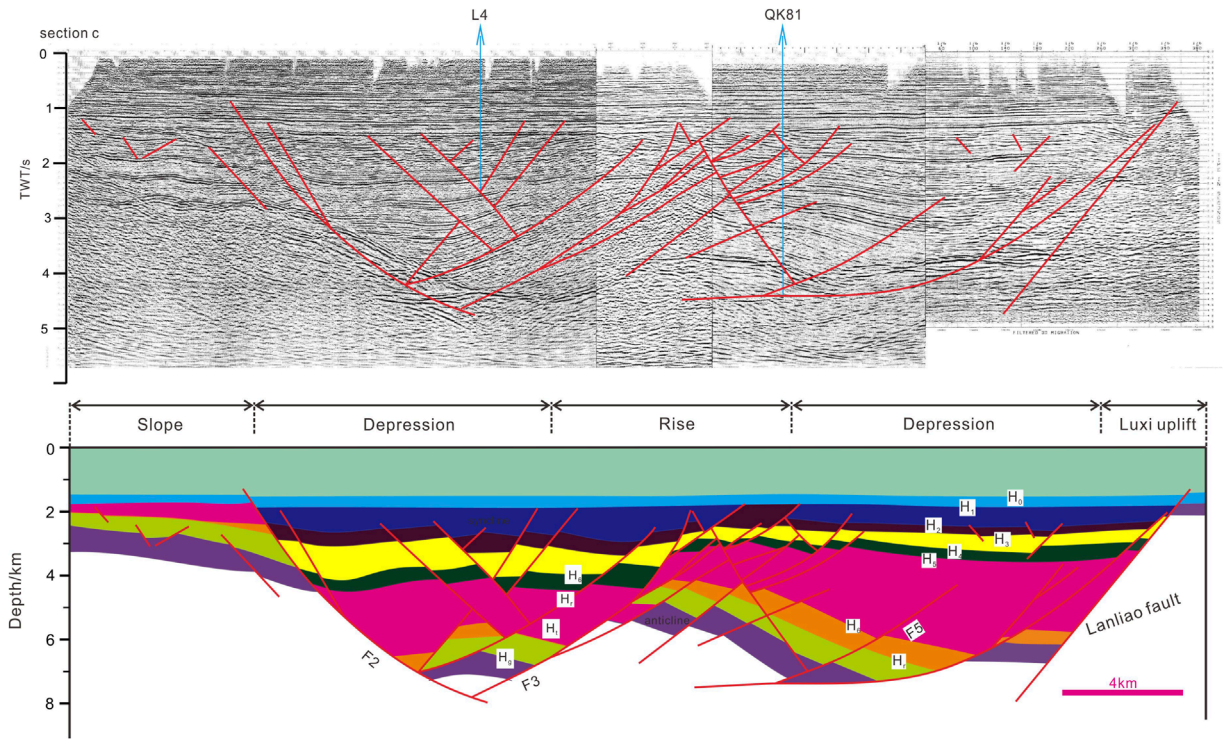

FIGURE 5
Seismic section c (upper) and interpreted (lower) geological profiles crosscut the middle Lanliao Fault (Figure 1 for location). TWT, two-way travel time.

also comprises the western limb of the aforementioned syncline (Figures 5–8). Both limbs of the anticlines are cut off by small faults, developing the asymmetric anticline geometry. In particular, intense faulting of fault F3 in Figures 7, 8 truncated the western limb of the anticline, forming an eastern dip monocline. These anticlines have developed to form the central rise in the middle and southern sag (Liu et al., 2001). The center rise serves as the horst, creating a graben–horst–graben structure between the west dipping fault F3 and east dipping fault F2 (Figures 7, 8). The reverse anticlines are only observed in the northern sag and, the central rise exists in the middle–southern sag (Figures 3–6).

Differences in kinematic characteristics are also reflected in the displacement and rifting period of the Lanliao Fault. This article uses seismic profiles and balanced cross section to demonstrate the extension of the Lanliao Fault in the Paleogene. The extension of the Lanliao Fault shows significant changes along its direction, with very obvious segmentation (Qi et al., 2006). During the Es_4 period, the southern fault was significantly larger than the middle part, while the sedimentary thickness in the north was extremely thin and showed little correlation with fault activity. The Es_3 period was the peak period of faulting. During this time, the extension displacement of the southern and middle segments was relatively large, while the extension displacement of the northern segment was relatively small.

The largest extension displacement migrates northward compared to the Es_4 period. In the Es_2 period, the displacement of the southern Lanliao Fault was significantly smaller than that of the middle segment. Extension displacement moved to other secondary faults in the southern Dongpu Sag, such as the Huanghe Fault and Changyuan Fault. Shortening rates from balanced cross section also confirm this point of view (Figure 10). The extension rate of the Lanliao Fault was the highest in the Es_3 period, at 36%, followed by the Es_2 period at 25%, while the Es_4 period had a relatively small extension rate of 20% (Liu, 2009).

4 Segmentation of the Lanliao Fault

Generally, large-scale normal faults consist of overlapped and piecewise fault segments, with sizes varying remarkably along the strike (Tchalenko, 1970; Machette et al., 1991; Gawthorpe and Leeder, 2000; Jackson et al., 2002; Peacock, 2002). Su et al. (2011) suggested three principles for distinguishing the segmentation of large normal faults: 1) strike and dip differences between fault segments; 2) sharp decreases in vertical fault throws and strata thicknesses at segment edges compared to the depocenter; and 3) patterns and locations of the transfer zone in the hanging wall. Fault segment identification primarily depends on vertical fault throw, layer thickness, and appearance of transfer zones, while changes in the fault strike and dip angle are secondary sources of evidence.

Fault displacement or throw refers to the distance between corresponding strata particles on the hanging wall and footwall after faulting (Jackson et al., 2002). Approximate values of the displacement could be acquired by measuring the vertical component of the total layer displacement on the seismic sections (Su et al., 2011). The Paleogene strata in the footwall of the Lanliao fault were not preserved due to denudation or non-deposition; therefore, throw variations along the strike could be obtained

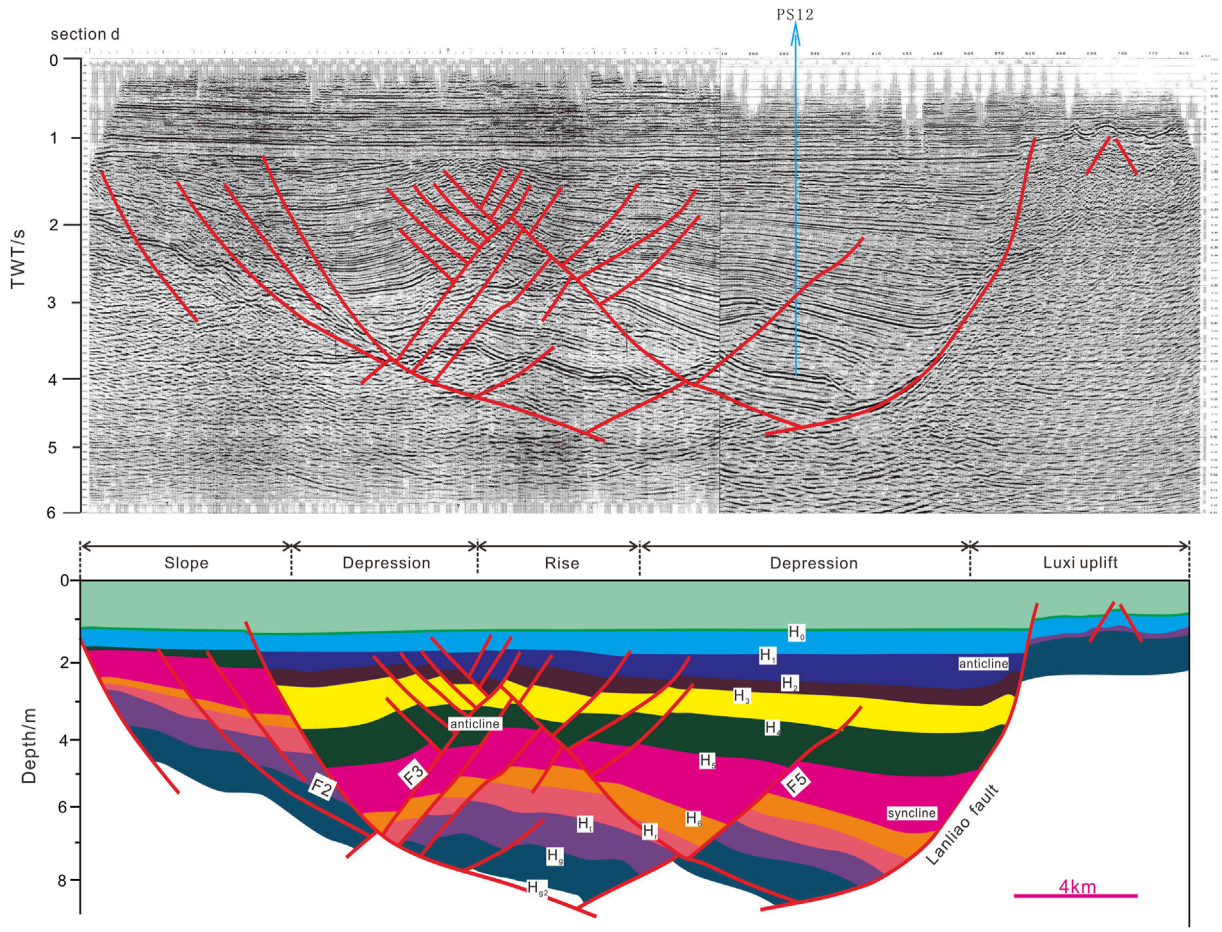

FIGURE 6
Seismic section d (upper) and interpreted (lower) geological profiles crosscut the middle Lanliao Fault (Figure 1 for location). TWT, two-way travel time.

by using the footwall H_1 horizon as a marker relative to each syn-rift sequence base (H_r–H_2) on the hanging wall. Variations in vertical fault throw and layer thickness with a strike distance could be portrayed in vertical throw-distance (Vt-d) and layer thickness-distance (Lt-d) profiles, as shown in Figure 11. Maxima and minima of fault throw and layer thicknesses have been applied to distinguish tips and centers of original fault segments, which would subsequently link to form a continuous boundary fault (Young et al., 2001). Using Vt-d and Lt-d profiles, five independent original fault segments have been identified from the Lanliao fault: the North fault segment (NFS), the Sinzhuang fault segment (SFS), the Qianliyuan fault segment (QFS), the Baimiao-Gegangji fault segment (BGFS), and the Mafang fault segment (MFS). The strikes and lengths of these segments are extracted from the structural sketch of reflection layer H_3. SFS's strike and length are 21° and 39 km ; NFS are 16° and 26 km; QFS are 32° and 58 km; BGFS are 42° and 15 km; and MFS are 17° and 55 km, respectively (Figure 11B).

Vt-d and Lt-d profiles also indicate larger displacement in the SFS and MFS than that in the NFS and BGFS. The Vt-d profile displays a primary displacement maximum and a secondary maximum in the MFS (Figure 11A). Maxima distribution suggests that the MFS formed probably by the linkage of two original sub-segments in the early period. The displacement of the NFS and the BGFS oscillates along the strike, with differences in the displacement between maxima and minima approximately over 200 ms TWT. The Vt-d feature of the QFS exhibits two symmetrical maxima in the early syn-rift stage and a single maximum in the later stage. The fact indicated the amalgamation of two early independent sub-segments into a unified original segment. Fault throw in the SFS is nearly symmetrical. The throw pattern of the NFS decreases and tapers off toward the north. One single throw maximum is observed during the Es_2 period, which possibly relates to the development of the isolated NFS depocenter, the Dongbei Subsag.

The kinematic features of segment endpoints are characterized by relatively small extensions near transfer zones. There are two major transfer zones along the Lanliao Fault (Liu et al., 2004; Sun et al., 2006). The northern transfer zone overlaps the NFS, serving as a synchronous transition slope between the boundary fault and fault F6. The southern transfer zone essentially equals the BGFS fault segment, which is a large synthetic transfer zone observed in the strike-parallel seismic profile (Figure 9). The type of this synthetic transfer zone is transverse-fold, developed between SFS and QFS. Faulting and fault-controlled subsidence within the transfer zone are notably weak, compared to areas outside the

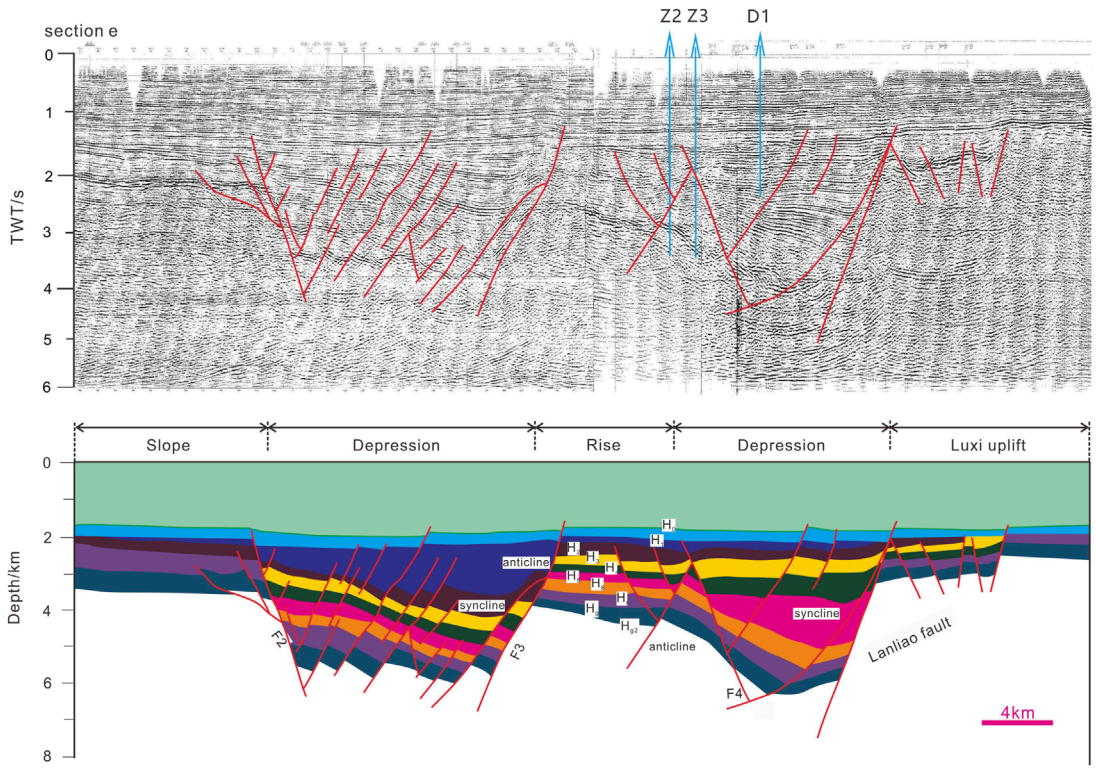

FIGURE 7
Seismic section e (upper) and interpreted (lower) geological profiles crosscut the middle Lanliao Fault (Figure 1 for location). TWT, two-way travel time.

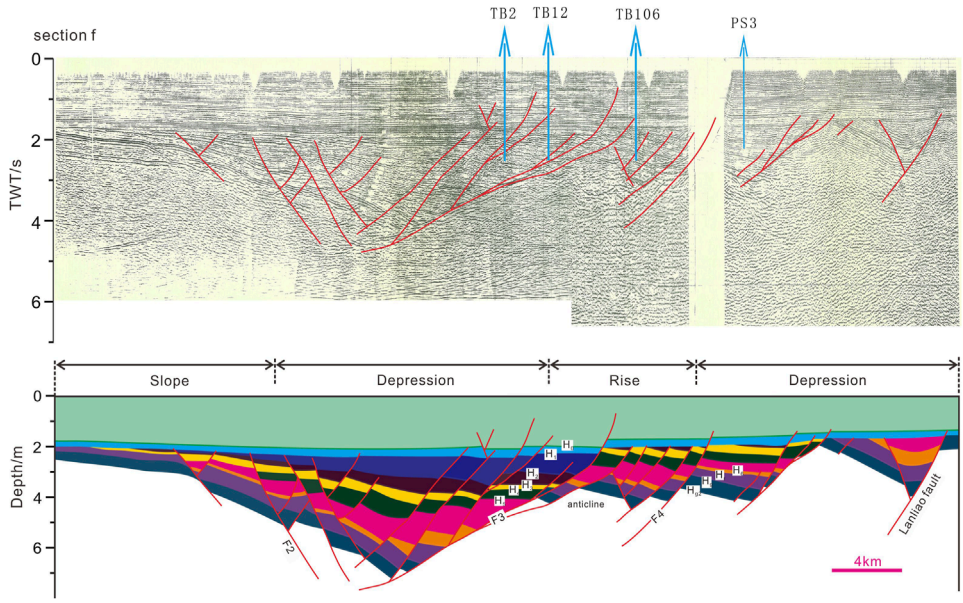

FIGURE 8
Seismic section f (upper) and interpreted (lower) geological profiles crosscut the southern Lanliao Fault (Figure 1 for location). TWT, two-way travel time.

transfer zone. Multiple small transverse faults develop parallel to the axis of a transverse fold in the transfer zone. These small faults terminate near the Lanliao Fault and may help regulate strain between different fault segments (Figure 9) (Chen et al., 2007; Cheng, 2009). Additionally, a small transverse anticline developed between MFS and SFS during Es_4 and early Es_3^3. Due to the early and

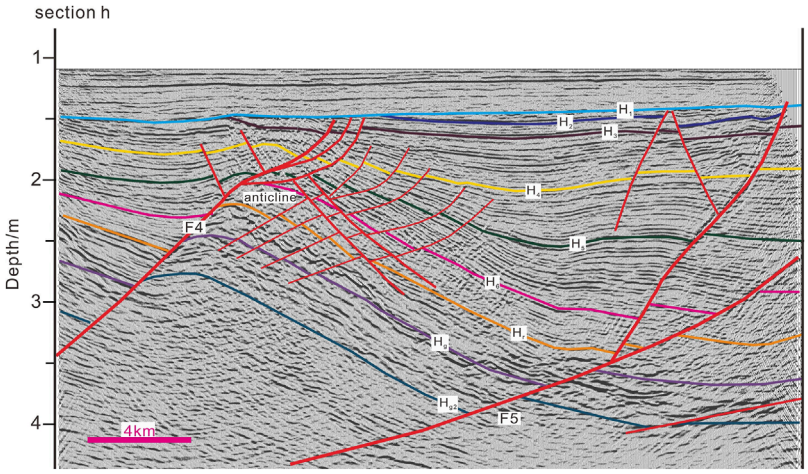

FIGURE 9
Seismic section g crosscut the southern Lanliao Fault (Figure 1 for location). TWT, two-way travel time.

weak fault activity and the thin sediments it controlled, the scale of this anticline is only approximately 2–3 km length, which is one-fifth of the BGFS (Sun et al., 2006; Sun, 2007).

5 Discussion

5.1 Linkage geometry

When fault segments converge, a transfer zone formed to regulate strain difference (Liu et al., 2000). Five segments of the Lanliao Fault shared approximate northwest dip; hence, only the synthetic transfer zone developed during the linkage of segments. As discussed above, the most commonly observed synthetic transfer zone comprises transverse anticlines (Liu et al., 2004). Transverse anticlines associated with boundary fault segments are common features, representing observable tips of fault segments correspond to the displacement minima (Morley, 2002). The displacement minima tend to remain constant during the linkage of fault segments. Five segments on the tip flank exhibit apparent differences in strike orientations and dip angles that constrain the overall slip within the fault zone. Although linked, displacement of each segment remains partially independent. Consequently, fragmented fault activities lead to the formation of the transfer zone in the tip zone.

MFS and QFS are the two major fault segments of the Lanliao Fault. These segments developed independently to form the Gegangji subsag and Qianliyuan subsag during the Es_4 and Es_3^3 periods (Figures 12A, B). During their linkage in Es_3^2, the need to adjust the significant strain difference between two segments resulted in the formation of a large transverse anticline, known as the BGFS. The formation of the BGFS adheres to the typical fault evolution geometry at synthetic transfer zones as detailed by Morley (2002). Throughout the basin's history, the development of a transverse anticline remains consistent due to significant differences in fault strike, dip angle, and activity strength (Figure 13A). Differences between the segments of the Lanliao fault are common. Transverse anticlines frequently occur between the linkage of NFS and QFS during Es_2 and the linkage of MFS and SFS during Es_3^1 (Figure 14).

Morley (2002) also proposed a special case of fault linkage. Once segments amalgamated, the new depocenter or displacement maximum on the fault zone may alter to fault joint where no significant geometry and strength difference between linking segments occur (Figure 13B). This scenario is exemplified by the linkage of two sub-segments to form the QFS on the Lanliao Fault. After the completion of the linkage during the Es_3^2 period, the QFS experienced slip along its entire length, dominating the Qianliyuan subsag (Figure 12D–G). The subsag developed overlaying the early transverse anticline in the control of the fault slip (Figure 15B).

5.2 Linkage and depocenter migration

The segmentation of the boundary fault has been investigated in detail; the next issue is the growth and linkage process of the boundary fault, which specifically includes two major problems: when did each fault segment link and the boundary fault finally join up? Moreover, how would the basin sediments respond during this process?

5.2.1 Linkage timing and sedimentary response

Determining the exact period of fault linkage is challenging; however, the process could be inferred from the Vt-d profile and the isopach map of the sedimentary sequence (Figures 11, 12). During the Es_4 deposition, faulting of the Lanliao fault was concentrated on the MFS, forming a significant depocenter. The MFS likely consisted of two initially isolated sub-segments, as evidenced by two displacement maxima in the Vt-d profile and two separated peaks in the isopach map (Figure 12). These two sub-segments were maintained independently in the early Es_4 and linked by the end of Es_4 (Figure 14). Concurrently, the SFS is developed, followed by the formation of a shallow depocenter.

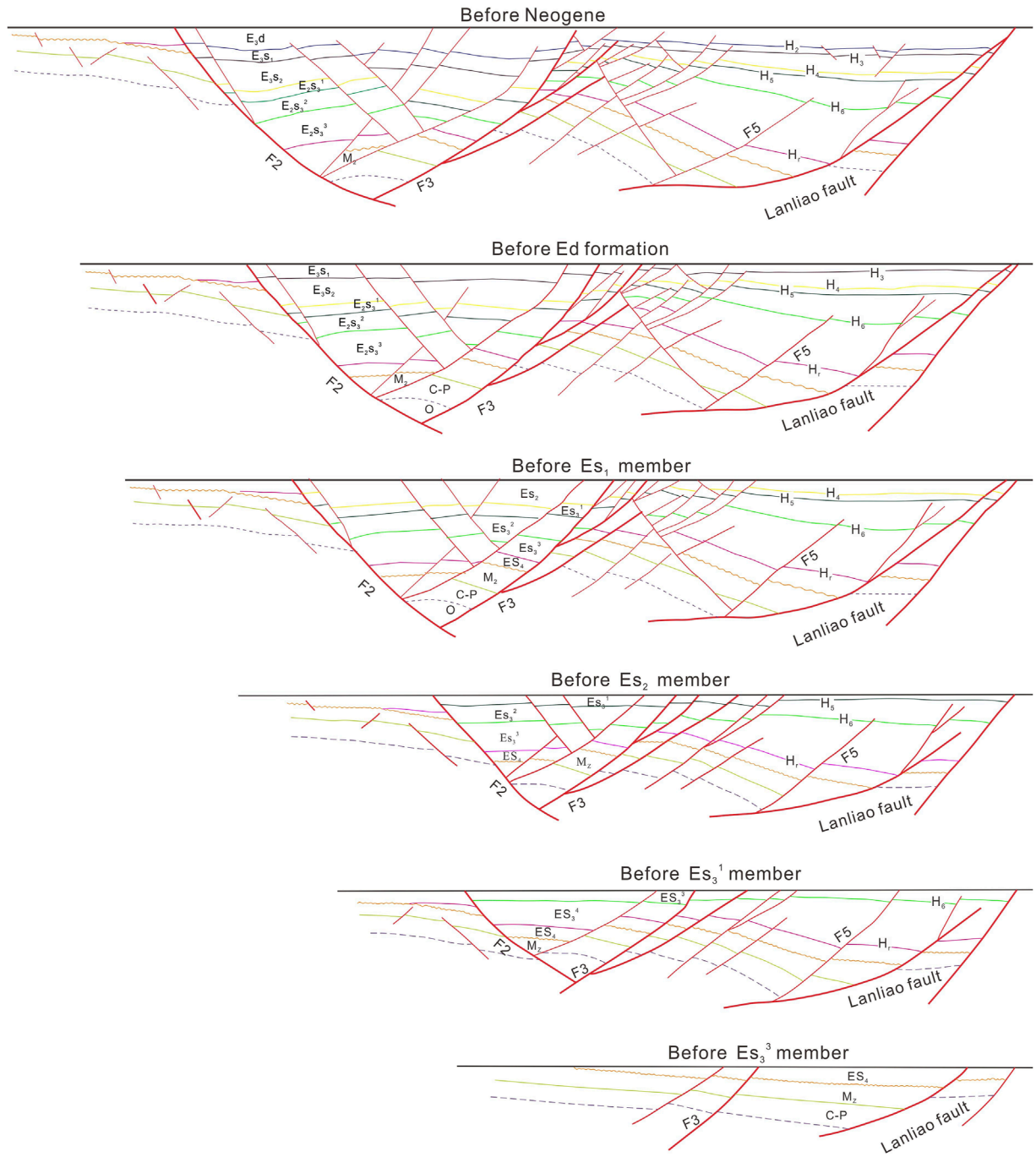

FIGURE 10
Balanced cross section of seismic profile c (modified after Liu, 2009).

Sedimentation typically responds to rifting morphology (Su et al., 2011). In the initial rift stage, the southern Gegangji subsag, controlled by the MFS, developed mudstone interlayered with gypsum rock, corresponding to deep lake faces. In contrast, the northern subsag, dominated by the SFS, accumulated sandstone interlayered with mudstone and siltstone under shallow to semi-lake faces. The differences in sediment lithology and facies indicate that the southern and northern Gegangji subsags were developed under a distinct sedimentary environment. This independent sedimentary environment also confirms the independent development of the MFS and SFS in the early Es_4 period.

Es_4 strata controlled by the NFS, QFS, and BGFS are relatively thin, indicating weak rifting. These fault segments correspond to "the early stage" of the boundary fault developed model, characterized by the poorly developed boundary fault with short strike extension (Morley et al., 2007). During this period, the SFS barely developed, as evidenced by very thin sediments, which are less than 100 m thick. The depocenter of the sag during the Es_4

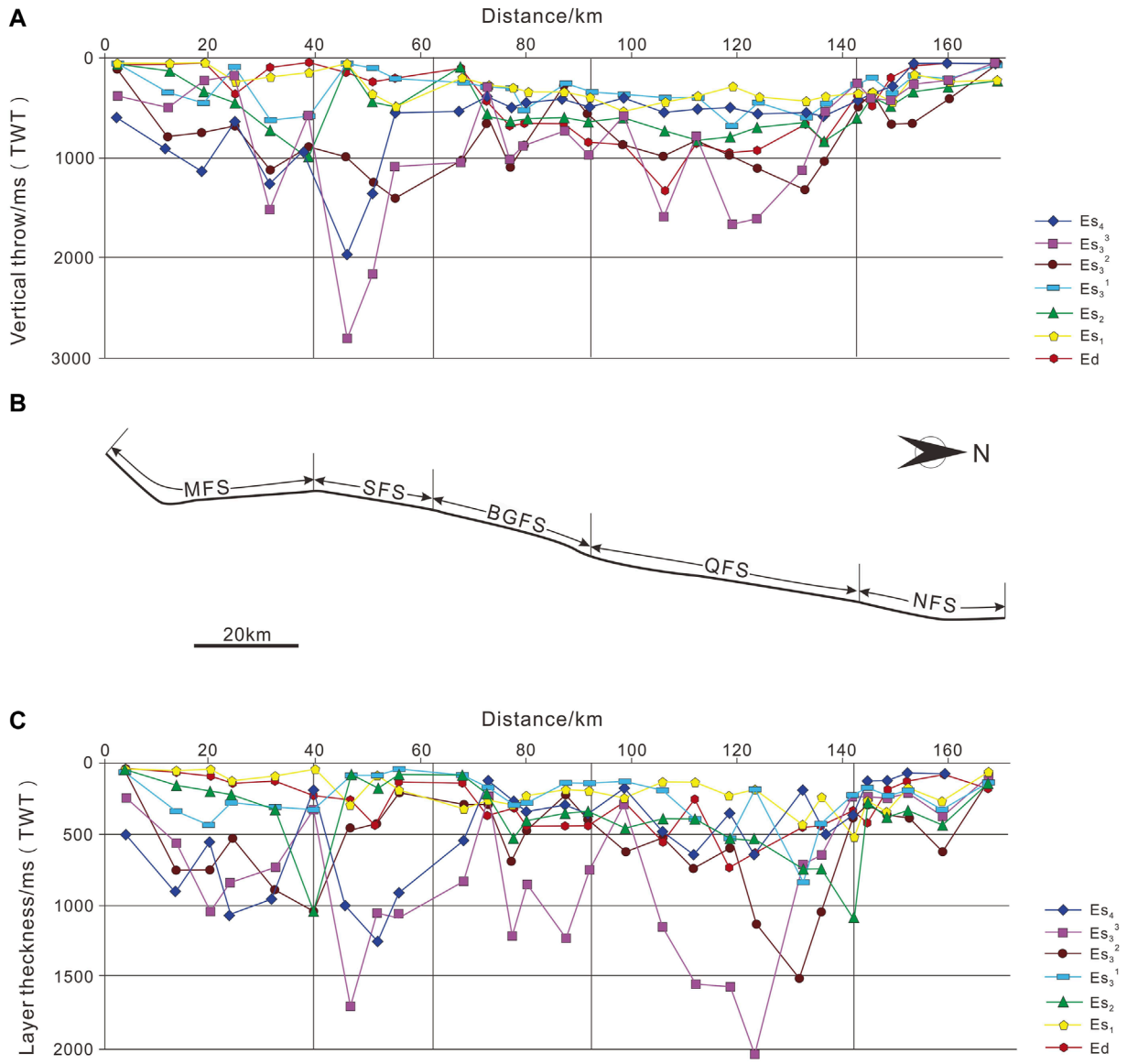

FIGURE 11
(A) Along-strike vertical throw vs. distance (Vt-d profile) for the bases of Es_4, Es_3^3, Es_3^2, Es_3^1, Es_2, Es_1, and Ed members, respectively. **(B)** Map view of the fault segments. **(C)** Along-strike thickness vs. distance (Lt-d profile) of each member.

period was located in the MFS with a maximum depth of 2,400 m, suggesting the most intensive fault activity (Figure 12).

During the Es_3^3 deposition, rifting continued to be prominent in the southern sag. The MFS controlled a strip-like joint depocenter along the fault zone (Figures 12, 13). Faulting in the SFS increased dramatically, resulting in maximum subsidence equals to that of the MFS. The connection of the MFS and SFS led to significantly intense tectonic subsidence, transitioning the Gegangji subsag into a semi-deep lake to a deep lake sedimentary environment. This environment favored the formation of widespread gravity-driven turbidite deposits distributed along the fault strike. Meanwhile, the QFS, NFS, and SFS still exhibited "the early stage." The evaporate deposits controlled by the arid and shallow water environment in the northern sag indicated weak and independent branch fault activities.

During the Es_3^3 period, the MFS remained the primary depocenter, reaching a maximum depth of 1,200 m. Additionally, the BGFS developed and controlled sediments up to 1,100 m deep.

During Es_3^2, the faulting of the MFS gradually weakened and the depocenter shrank. The SFS kept developing (Figure 12C). Seismic profiles indicate that the QFS has already developed before Cenozoic, as proved by the thickness difference in the middle Triassic layer ($H_{1\text{-}2}$) between horizon H_r to H_t of the hanging wall and footwall (Figures 5, 6). The isopach map of the Es_3^2 member along the near NE–SW trending QFS shows two peaks, which means that the QFS also consists of northern and southern sub-segments (Figure 14). Although depocenters of the southern QFS and SFS were not entirely superimposed completely by the end of Es_3^2 deposition, the migration of subsidence maxima was confined

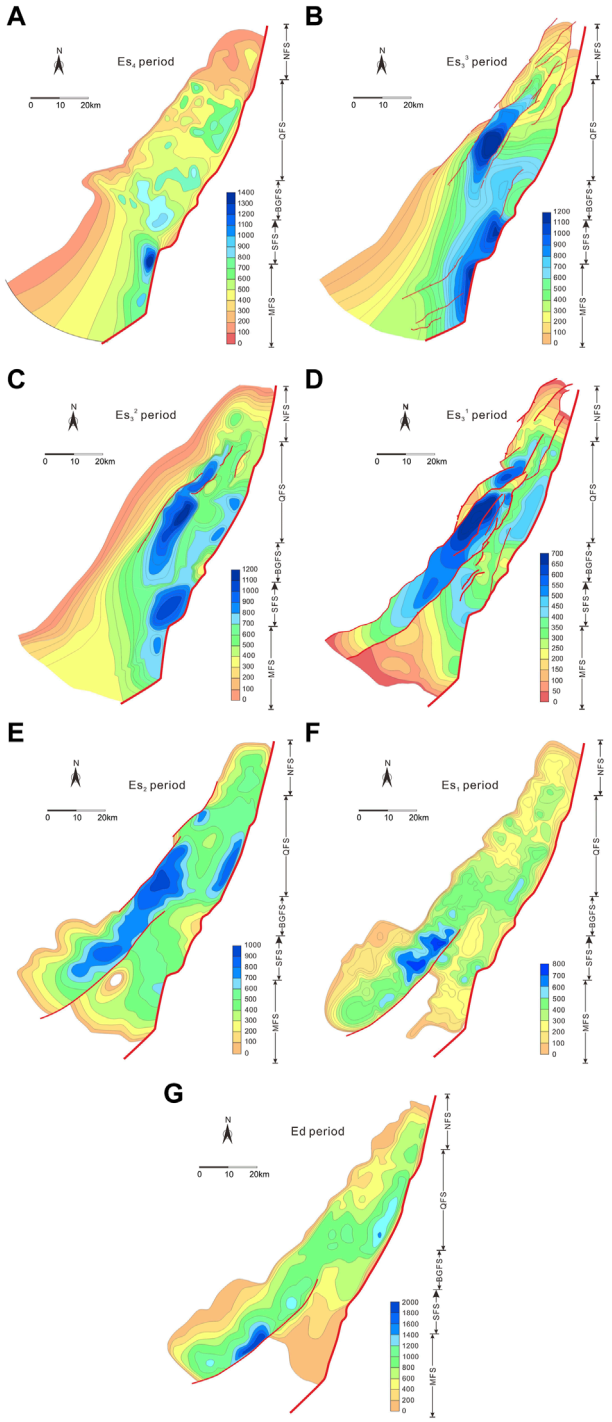

FIGURE 12
Contour maps of the basin subsidence from Es4 to Ed period, the unit of scale in the right corner is in meters.

within the fault segment. Accordingly, stationary segment tips of the southern QFS and MFS constantly developed in a stable site, resulting in a large transverse anticline, the BFGS segment. The BFGS became the new solo depocenter along the Lanliao Fault, controlling 1000 m sediments.

During Es_3^1, the strata controlled by the MFS and SFS gradually evolved into a slope pattern due to the weakening of rifting activities (Figure 12D). Two initially sub-segments of the QFS eventually linked and merged into a unified depocenter, dominating the Lanliao Fault with 450-m sediments. The rifting activity in the Dongpu Sag reached its peak in the early Es_3 period and then weakened by Es_3^1, as evidenced by the reduced thickness of tectonic subsidence (Figure 14). During this time, the sedimentary water levels became shallower and the lake basins gradually shrank. Saline lake and gravity turbidite deposits basically dissolved, and the sedimentary facies converted into over lake and fluvial facies (Tang and Wang, 2008).

During the deposition of the Es_2 member, the southern part of the boundary fault, including the MFS, SFS, and BGFS, was largely inactive. In contrast, the QFS maintained intense rifting and sedimentation, accumulating over 900 m of deposits. NFS formed an observable secondary depocenter along the Lanliao Fault, and subsidence isopach patterns indicated the linkage of the NFS and QFS (Figure 12E). By the end of the Es_2 period, five segments of the Lanliao Fault have completed interconnection (Figure 14). Corresponding to the weakened faulting and deposition in the southern sag, sediments inside the basin were mainly fluvial faces. Nevertheless, the incremental linkage of the QFS and NFS in the northern sag resulted in the expansion of the lake basin and the development of a deep-water lacustrine environment. The sedimentary formations in this region are composed of mudstone, argillaceous stone, and mudstone interlayered with gypsum. This sedimentary pattern reflects the ongoing tectonic activity in the northern fault, which promoted the formation of a deep lacustrine environment despite the overall reduction in rifting intensity in the southern fault.

5.2.2 Basin depocenter migration

Long-lived boundary faults like the Lanliao Fault (over 10 m.y.) generally exhibit variable maximal fault displacement sites that relocate from one part of the fault to another over time. The Lanliao Fault shows a frequent change in the location of Eocene and Oligocene depocenters. These fault segments play a crucial role in controlling the relocation of depocenters and the distribution of sediments. Initially, faulting is concentrated in the southern part. The southern segments, MFS and SFS, formed a graben depocenter of the Es_3^3–Es_3^2 member known as the Gegangji subsag. As the fault segments propagate northward, they often weaken or become abandoned, with sedimentation attenuating correspondingly. In the Es_3^1 member, the depocenter migrates northward due to the saltatory propagation of fault segments, accompanied by material filling and deposition. Consequently, a half-graben style Qianliyuan subsag was formed (Figures 12, 14). During the Es_2 period, the northward propagation of the Lanliao fault resulted in the development of the isolated NFS depocenter, the Dongbei subsag.

The relocation of maximal displacement and the depocenter was saltatory rather than progressive. The jump appears to be abrupt as the existing transverse fold remains stable, and no transitional structure is observed. Had depocenter moved northward progressively across the BGFS, the transverses anticline should have become a depocenter as well. The abandoned fault

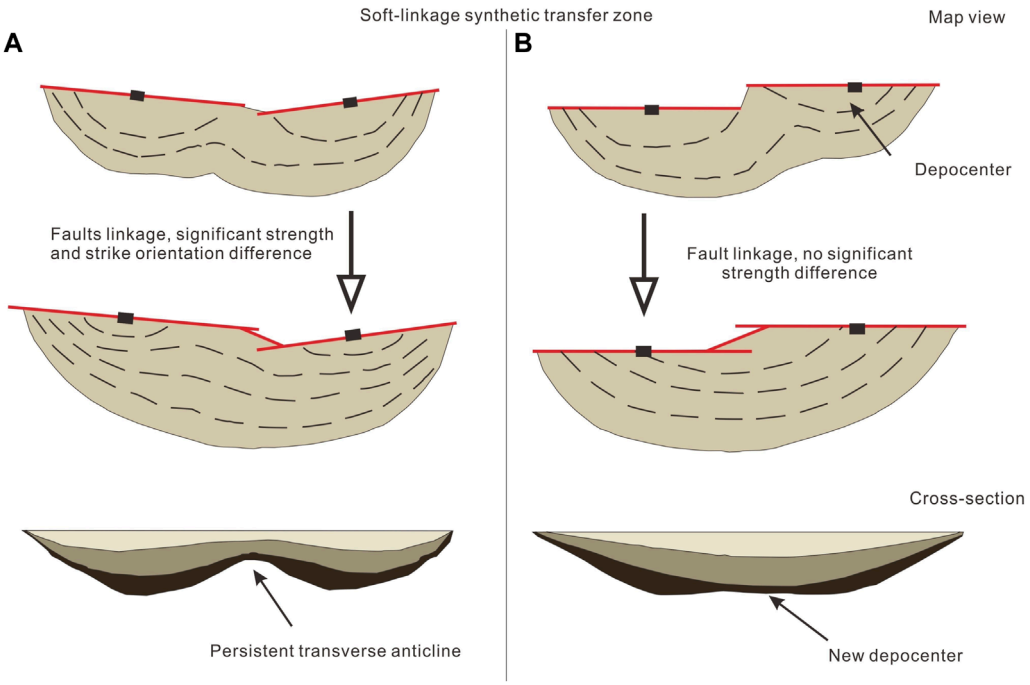

FIGURE 13
Schematic evolution of faults amalgamated at a synthetic transfer zone (modified from Morley, 2002). **(A)** The old displacement patterns may prevail throughout the basin history when fault segments link with significant strength and strike orientation differences; **(B)** once joined, former transverse anticline on the fault zone may alter so as to control a new depocenter lies at the approximate center of the newly amalgamated fault.

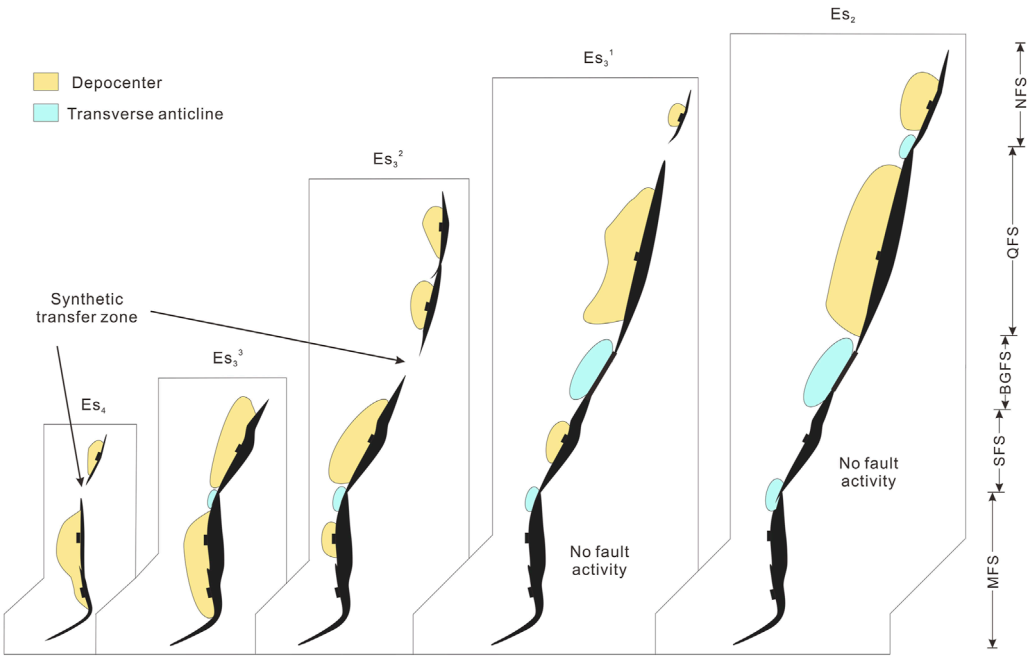

FIGURE 14
Fault linkage, depocenters, and transverse folds showing the evolution of the Dongpu Sag.

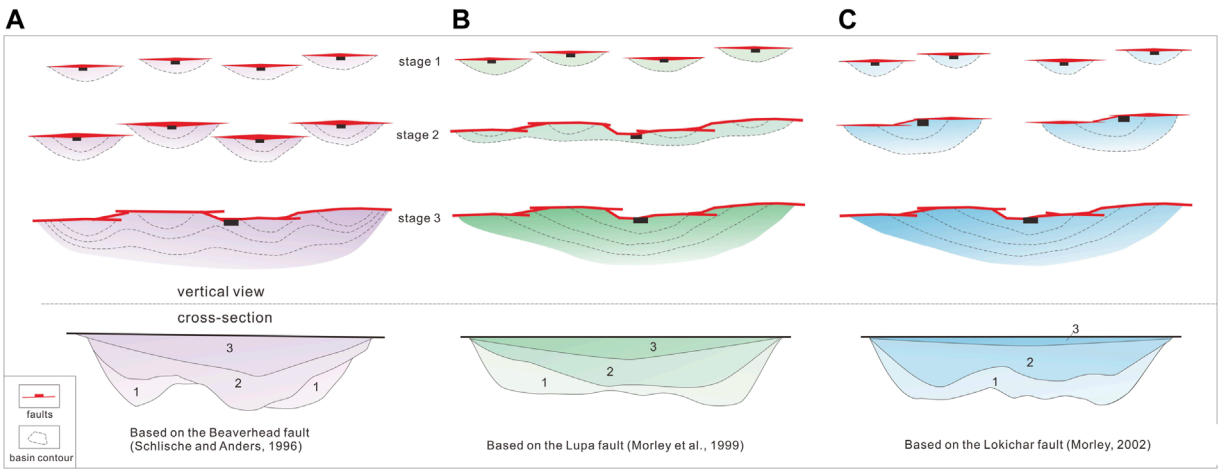

FIGURE 15
Sketch of basic models for boundary fault propagation and depocenter development during and **(A)** after minor faulting has created an extensive area of subsidence (Schlische and Anders, 1996), **(B)** prior to significant basin formation (Morley, 1999), and **(C)** along with basin development (Morley, 2002)

segment of the MFS hanging wall was partially eroded during the Oligocene (Figure 8).

5.3 Linkage pattern

We further look forward to investigating the geometric pattern of the boundary fault linkage. A key issue is what the typical linkage geometry of the Lanliao fault is. Three models detailing the growth and linkage of boundary faults have been proposed: 1) small faults develop independently and create extensive areas of subsidence, respectively. The linkage of small faults occur at the later syn-rift stage, and the boundary fault develops relatively late in the basin evolution, lacking general controlling on the basin geometry and sedimentation. A representative of this linkage pattern is Usangu Flats in Tanzania (Figure 15A) (Ebinger et al., 1989; Anders and Schlische, 1994; Fontijn et al., 2010). 2) During the early syn-rift stage, the rapid fault linkage forms a boundary fault prior to significant basin development. Once linked, the boundary fault maintains the strike length and only increases fault displacement to dominate the development of basin deposits, which is represented by East Kigoma fault, Lake Tanganyika, North Africa (Figure 15B) (Morley, 1999). 3) The length of the boundary fault increases by the lateral propagation of small faults accompanied with simultaneous material filling and deposition. Boundary fault propagation occurs during the development of a basin, such as the Lokichar Fault in Kenya (Figure 15C) (Schlische, 1991; Morley, 2002; Macgregor, 2014).

The Lokichar Fault is a large normal fault developed in the East African rift system (Morley, 1999; Morley, 2002). During the Paleogene and early Miocene, the southern Lokichar Fault formed through the connection of two initially independent faults. The southern fault was active relatively early in the basin history and deactivated later in favor of northern fault segments activity during the late Miocene and Pliocene. The northern and southern faults were separated by a synthetic transfer zone. Later, the two faults became linked across the transfer zone. Morley suggested that the Lokichar Fault is a representative of a pattern (3).

Reviewing the linkage history of the Lanliao Fault, we observed a similarity with the Lokichar Fault. During the early Eocene, the early independent MFS and SFS linked to form the southern part of the Lanliao Fault, leading to the rapid development of the depocenter known as the Gegangji subsag. In the late Eocene, the southern MFS and SFS deactivated, while the independent QFS formed to control the Qianliyuan subsag. By the end of the Eocene, the SFS and QFS became linked across the synthetic transfer zone (BGFS), showing a similar evolution pattern to that of the Lokichar Fault.

5.4 Post-linkage development

There are two branches on the post-linkage development of boundary faults: 1) maximum displacement maintains around the center of the boundary fault (Morley, 2002); and 2) the post linkage development of the boundary fault could also induce the obvious relocation of the depocenter (Allen and Allen, 2013). The initiation of F2 was later than the Lanliao Fault. Once formed during Es_3, subsidence controlled by F2 was equal to that controlled by the MFS of the Lanliao Fault (Figures 12B–D). During the Es_3^2–Es_2 period, fault displacement and subsidence of F2 literally exceeded the boundary fault, developing into the depocenter and controlling the Mengmangji subsag.

Large normal fault activity may end abruptly due to a major external event, such as tectonic inversion, or gradually weaken as other faults nearby increase the rifting intensity of the boundary fault (Twiss and Moores, 2007; Allen and Allen, 2013). According to the faulting history of the Dongpu Sag, two possible candidates of activity succession to induce the boundary fault to weaken are faults F2 and F3. The faulting maximum of the Lanliao fault was during Es_4–Es_2 and that of F2 was during Es_3–Es_2. The QFS fault segment and fault F2 both maintained prosperity during Es_2; subsidence declined swiftly, and the depocenter shrunk during

the Es_1 (Figure 12F). This indicates that the extension of F2 and that the boundary fault shows a simultaneous feature. Generally, the formation of F2 is more likely an associated antithetic fault accommodating the huge shovel extension of the Lanliao Fault, rather than a fault succeeding the displacement. Shovel fault patterns of the Lanliao Fault lead to an issue that the rollover of the hanging wall could not bear such a significant extension in Es_3, thereby forming antithetic adjusting faults to the west or possibly forming a ramp-flat extensional duplex in depth (Qi et al., 2006; Cheng et al., 2010; Xu et al., 2018).

Stretching of the Lanliao Fault and fault F2 died out during Es_1, followed by shrank of subsidence. Therefore, the Es_1 deposition is believed to be an intermittent of episodic rifting in the Bohai Bay Basin (Qi, 2004; Luo et al., 2015; Zuo et al., 2017). During Es_1–Ed, the major active fault was fault F3. F3 formed during Es_3^1 and was strongly activated during Es_1–Ed later than F2. Rifting of F3 was very intense in Oligocene, subsiding over 2,000 m in the Menggangji subsag; and the footwall uplifted and eroded heavily (Figure 12G). Considering the strike and dip similarity of the boundary fault and F3, as well as the continuity in geological time, it is possible that F3 was the successive fault that occupied the displacement of the Lanliao Fault during Es_1–Ed.

6 Conclusions

Based on the seismic data, we studied the evolution of the boundary fault of the Dongpu Sag, Bohai Bay Basin, on the fault deformation and displacement. The vertical throw-distance (Vt-d) and layer thickness-distance (Lt-d) profiles, as well as the site of transverse fold, strike orientation, and dip angel variations, suggest that the single Lanliao Fault is evolved by the approach, interaction, and amalgamation of early isolated fault segments. These fault segments are MFS, SFS, BGFS, QFS, and NFS, from south to north. By the end of the Es_4 period, MFS and SFS formed and linked. The QFS formed and joined to the SFS although the BGFS served as an intrabasin high or transverse anticline by Es_3^2. The formation and linkage of the NFS to QFS represents the final interconnection of the Lanliao Fault in Es_3^1.

The linkage of the Lanliao Fault and the deposition of the Dongpu Sag occur during the development of the basin, characterized by the saltatory lateral propagation of small fault segments accompanied by simultaneous material filling and sedimentation. Nearly all fault segment linkage abides by the synthetic transfer zone geometry that transverse anticline persists when segments with significant strength and strike differences are linked, represented by the linkage of the QFS and the SFS to form the BGFS. Only the linkage of the two sub-segments to form the QFS follows the geometry that fault joint becomes the new depocenter or displacement maximum with similar strength and strike orientations.

The Lanliao Fault died out during the Oligocene. In the late Oligocene (Ed), fault F3 shares similar strike and dip with the boundary fault, possibly occupied the displacement of the Lanliao Fault and is persistent throughout the post-linkage basin history, dominating basin geometry and sediment formation.

Data availability statement

The original contributions presented in the study are included in the article/Supplementary Material; further inquiries can be directed to the corresponding author.

Author contributions

HX: data curation, formal analysis, and writing–original draft. LQ: writing–review and editing. D-PY: writing–review and editing. X-WW: writing–review and editing.

Funding

The authors declare that financial support was received for the research, authorship, and/or publication of this article. This study was funded by the General Program of National Natural Science Foundation of China (Grant No. 42372263) and the Open Foundation of Collaborative Innovation Center for Wetland Conservation and Green Development of Hebei Province (No. 2024hbxczx3-2).

Conflict of interest

The authors declare that the research was conducted in the absence of any commercial or financial relationships that could be construed as a potential conflict of interest.

Publisher's note

References

Allen, A., and Allen, R. (2013). *Basin analysis: principles and application to petroleum play assessment*. Third edition. Chi Chester: Wiley-Blackwell.

Allen, M. B., Macdonald, D. I. M., Xun, Z., Vincent, S. J., and Brouet-Menzies, C. (1997). Early Cenozoic two-phase extension and late Cenozoic thermal subsidence and inversion of the Bohai basin, northern China. *Mar. Petrol. Geol.* 14, 951–972. doi:10.1016/S0264-8172(97)00027-5

Anders, M. H., and Schlische, R. W. (1994). Overlapping faults, intrabasin highs, and the growth of normal faults. *J. Geol.* 102, 165–179. doi:10.1086/629661

Chen, J., Li, S., Xiong, Y., and Bi, Y. (1998). Multiple petroleum systems in Tertiary extensional basins, East China: a case study of the Gunan–Fulin Basin. *J. Petroleum Geol.* 21, 105–118. doi:10.1111/j.1747-5457.1998.tb00648.x

Chen, S., Qi, J., Wang, D., Cheng, X., and Zhao, Y. (2007). Fault systems and transfer structures in Dongpu Sag. *Acta Pet. Sin.* 28 (1), 43–49. (in Chinese with English abstract). doi:10.3321/j.issn:0253-2697.2007.01.008

Cheng, X. (2009). The structural style in Dongpu sag, henan. *Geoscience* 23, 414–422. (in Chinese with English abstract). doi:10.3969/j.issn.1000-8527.2009.03.005

Cheng, X., Chen, F., Qi, J., et al. (2010). Evolutional impacts of extensional linkage fault system in Dongpu sag. *Geoscience* 24, 735–743. doi:10.3969/j.issn.1000-8527.2010.04.012

Ebinger, C. J., Deino, A. L., Drake, R. E., and Tesha, A. L. (1989). Chronology of volcanism and rift basin propagation: rungwe volcanic province, East Africa. *J. Geophys. Res.* 94 (15), 15785–15803. doi:10.1029/JB094iB11p15785

Fontijn, K., Delvaux, D., Ernst, J., Kervyn, M., Mbede, E., and Jacobs, P. (2010). Tectonic control over active volcanism at a range of scales: case of the Rungwe Volcanic Province, SW Tanzania; and hazard implications. *J. Afr. Earth Sci.* 58 (5), 764–777. doi:10.1016/j.jafrearsci.2009.11.011

Fossen, H., and Rotevatn, A. (2016). Fault linkage and relay structures in extensional settings-A review. *Earth-Science Rev.* 154, 14–28. doi:10.1016/j.earscirev.2015.11.014

Gawthorpe, R. L., and Leeder, M. R. (2000). Tectono-sedimentary evolution of active extensional basins. *Basin Res.* 12, 195–218. doi:10.1111/j.1365-2117.2000.00121.x

He, L., and Wang, J. (2003). Cenozoic thermal history of the Bohai Bay Basin: constraints from heat flow and coupled basin–mountain modeling. *Phys. Chem. Earth.* 28 (9–11), 421–429. doi:10.1016/S1474-7065(03)00062-7

Higgins, S., Davies, J. D., and Clarke, B. (2007). Antithetic fault linkages in a deep water fold and thrust belt. *J. Struct. Geol.* 29, 1900–1914. doi:10.1016/j.jsg.2007.09.004

Hou, G., and Hari, R. (2014). Mesozoic-Cenozoic extension of the bohai sea: contribution to the destruction of north China craton. *Front. Earth Sci.* 8, 202–215. doi:10.1007/s11707-014-0413-3

Huang, L., Liu, C., Wang, Y., Zhao, J., and Mountney, P. (2014). Neogene quaternary post-rift tectonic reactivation of the bohai bay basin, eastern China. *AAPG Bull.* 98 (7), 1377–1400. doi:10.1306/03071413046

Jackson, C. A., GawthorpeL, R., and Sharp, I. R. (2002). Growth and linkage of the East Tanka fault zone, Suez rift: structural style and syn-rift stratigraphic response. *Geol. Soc. Lond.* 159, 175–187. doi:10.1144/0016-764901-100

Ji, H., Li, S., Greenwood, P., Zhang, H., Pang, X., Xu, T., et al. (2018). Geochemical characteristics and significance of heteroatom compounds in lacustrine oils of the Dongpu Depression (Bohai Bay Basin, China) by negative-ion Fourier transform ion cyclotron resonance mass spectrometry. *Mar. Petroleum Geol.* 97, 568–591. doi:10.1016/j.marpetgeo.2018.07.035

Li, B., Yu, C., Zhao, Y., Wu, Y., Xin, Y., and Guo, Y. (2023). Tectonic evolution of the Gubei sag with multiple boundary faults in the Bohai Bay Basin, East China and the control of tectonics over paleo-structures and hydrocarbons: insights from three-dimensional reconstructions. *J. Asian Earth Sci.* 256, 105817. doi:10.1016/j.jseaes.2023.105817

Li, J., Liu, Z., Liu, J., Chen, L., Liu, H., Huang, L., et al. (2021a). Transformation of sediment delivery and dispersal patterns controlled by relay-ramp evolution along the boundary fault of a lacustrine rift: the Eocene Shahejie formation, Dongying Sag, Bohai Bay Basin, NE China. *Mar. Petroleum Geol.* 128, 105044. doi:10.1016/j.marpetgeo.2021.105044

Li, S., Pang, X., Li, M., Jin, Z., Qiu, Q., and Gao, Y. (2005). Geochemistry of petroleum systems in the Niuzhuang south slope of Bohai Bay Basin: Part 4, evidence for new exploration horizons in a maturely explored petroleum province. *Org. Geochem.* 36, 1135–1150. doi:10.1016/j.orggeochem.2005.03.004

Li, T., Zhang, Y., Lu, R., Gao, J., Sun, J., Zhao, X., et al. (2021b). 3D geometry of the Lanliao Fault revealed by seismic reflection profiles: implications for earthquake clustering in the Dongpu Sag, North China. *Tectonophysics* 806, 228798. doi:10.1016/j.tecto.2021.228798

Liang, J., Wang, L., Bai, Y., Ji, X., and Duo, X. (2016). Cenozoic tectonic evolution of the bohai Bay Basin and its coupling relationship with Pacific plate subduction. *J. Asian Earth Sci.* 127, 257–266. doi:10.1016/j.jseaes.2016.06.012

Liu, D., Ding, G., and Lu, B. (2001). Genesis model of hanging wall syncline and intermediate Uplift of extensional fault. Science in China. *Earth Sci.* 31, 985–991. (in Chinese with English abstract). doi:10.3321/j.issn:1006-9267.2001.12.003

Liu, J. (2009). *The structural framework of Dongpu depression*. Doctoral Dissertation.

Liu, J., Wang, X., and Wang, W. (2004). Transition structures in linqing depression. *Geol. Sci. Technol. Inf.* 23 (4), 51–54. doi:10.3969/j.issn.1000-7849.2004.04.011

Liu, J., Wang, X., and Zhou, Z. (2000). Research advance in transition structure in extended region. *Geol. Sci. Technol. Inf.* 19 (3), 27–32. (in Chinese with English abstract). doi:10.3969/j.issn.1000-7849.2000.03.006

Liu, Y., Chen, Q., Wang, X., Hu, K., Cao, S., Wu, L., et al. (2017). Influence of normal fault growth and linkage on the evolution of a rift basin: a case from the Gaoyou depression of the Subei Basin, eastern China. *AAPG Bull.* 101 (2), 265–288. doi:10.1306/06281615008

Lu, K. Z., and Qi, J. F. (1997). *Tectonic model of cenozoic petroliferous basin Bohai Bay Province (in Chinese)*. Beijing, China: Geological Publishing House, 3–5.

Lucas, L., Vasconcelos, D., Balsamo, F., Silva, M., Nogueira, F., Stohler, R., et al. (2023). Interaction and linkage of basin-boundary fault segments control deformation bands distribution and damage zone permeability. *J. Struct. Geol.* 176, 104958. doi:10.1016/j.jsg.2023.104958

Luo, Y., Zhao, Y., Chen, H., and Hui, U. (2015). Fracture characteristics under the coupling effect of tectonic stress and fluid pressure: a case study of the fractured shale oil reservoir in liutun subsag, Dongpu sag, Bohai Bay Basin, eastern China. *Petroleum Explor. Dev.* 42 (2), 196–205. doi:10.1016/S1876-3804(15)30006-9

Macgregor, D. (2014). History of the development of the East African Rift System: a series of interpreted maps through time. *J. Afr. Earth Sci.* 101, 232–252. doi:10.1016/j.jafrearsci.2014.09.016

Machette, M., Personius, S. F., Nelson, A. R., Schwartz, D. P., and Lund, W. R. (1991). The Wasatch fault zone, Utah—segmentation and history of Holocene earthquakes. *J. Struct. Geol.* 13, 137–149. doi:10.1016/0191-8141(91)90062-N

McLeod, A. E., Dawers, N. H., and Underhill, J. R. (2000). The propagation and linkage of normal faults; insights from the Strathspey-Brent-Statfjord fault array, northern North Sea. *Basin Res.* 12, 263–284. doi:10.1111/j.1365-2117.2000.00124.x

Morley, C. K. (1999). Patterns of displacement along large normal faults: implications for basin evolution and fault propagation based on examples from East Africa. *AAPG Bull.* 83, 613–634. doi:10.1306/00AA9C0A-1730-11D7-8645000102C1865D

Morley, C. K. (2002). Evolution of large normal faults: evidence from seismic reflection data. *AAPG Bull.* 86, 961–978. doi:10.1306/61EEDBFC-173E-11D7-8645000102C1865D

Morley, C. K., Gabdi, S., and Seusutthiya, K. (2007). Fault superimposition and linkage resulting from stress changes during rifting: examples from 3D seismic data, Phitsanulok Basin, Thailand. *J. Struct. Geol.* 29, 646–663. doi:10.1016/j.jsg.2006.11.005

Peacock, D. (2002). Propagation, interaction and linkage in normal fault systems. *Earth-Science Rev.* 58, 121–142. doi:10.1016/S0012-8252(01)00085-X

Phoosongsee, J., and Morley, C. (2019). Evolution of a major extensional boundary fault system during multi-phase rifting in the Songkhla Basin, Gulf of Thailand. *J. Asian Earth Sci.* 172, 1–13. doi:10.1016/j.jseaes.2018.08.028

Qi, J. (2004). Two tectonic systems in the cenozoic Bohai Bay Basin and their genetic interpretation. *Chin. Geol.* 31 (1), 15–22. (in Chinese with English abstract).

Qi, J., Wang, D., Chen, S., et al. (2006). Impact of geometry and kinematics of Lanliao fault on structural styles in Dongpu sag. *Oil Gas Geol.* 27 (4), 451–459. (in Chinese with English abstract). doi:10.11743/ogg20060403

Qi, J., and Yang, Q. (2010). Cenozoic structural deformation and dynamic processes of the Bohai Bay basin province, China. *Mar. Petroleum Geol.* 27, 757–771. doi:10.1016/j.marpetgeo.2009.08.012

Ren, J., Tamaki, K., Li, S., and Zhang, J. (2002). Late Mesozoic and Cenozoic rifting and its dynamic setting in Eastern China and adjacent areas. *Tectonophysics* 344 (3-4), 175–205. doi:10.1016/S0040-1951(01)00271-2

Ren, J. S. (1996). The continental tectonics of China. *J. Southeast Asian Earth Sci.* 13 (3–5), 197–204. doi:10.1016/0743-9547(96)00026-8

Schlische, R. W. (1991). Half-graben basin filling models: new constraints on continental extensional basin development. *Basin Res.* 3, 123–141. doi:10.1111/j.1365-2117.1991.tb00123.x

Schlische, R. W., and Anders, M. H. (1996). "Stratigraphic effects and tectonic implications of the growth of normal faults and extensional basins," in *Reconstructing the history of basin and range extension using sedimentology and stratigraphy*. Editor K. K. Beratan (Geological Society of America Special Publication), 303, 183–203. doi:10.1130/0-8137-2303-5.183

Shao, X., Pang, X., Li, H., Hu, T., Xu, T., Xu, Y., et al. (2018). Pore network characteristics of lacustrine shales in the Dongpu Depression, Bohai Bay Basin, China, with implications for oil retention. *Mar. Petroleum Geol.* 96, 457–473. doi:10.1016/j.marpetgeo.2018.06.015

Shi, B., Wu, Z., Wang, J., Zhou, Y., and Dai, Q. (1999). A study on the geological characteristics and geodynamic origin of Dongying movement, bohai bay basin. *Exp. Pet. Geol.* 21 (3), 196–200. doi:10.3969/j.issn.1001-6112.1999.03.002

Soliva, R., and Benedicto, A. (2004). A linkage criterion for segmented normal faults. *J. Struct. Geol.* 26, 2251–2267. doi:10.1016/j.jsg.2004.06.008

Su, J., Zhu, W., Lu, H., Xu, M., Yang, W., and Zhang, Z. (2009). Geometry styles and quantification of inversion structures in the Jiyang depression, Bohai Bay Basin, eastern China. *Mar. Petroleum Geol.* 26, 25–38. doi:10.1016/j.marpetgeo.2007.08.003

Su, J., Zhu, W., Wei, J., Xu, L., Yang, Y., Wang, Z., et al. (2011). Fault growth and linkage: implications for tectonosedimentary evolution in the chezhen basin of bohai bay, eastern China. *AAPG Bull.* 95, 1–26. doi:10.1306/06301009207

Su, Y., Li, Q., Tian, Y., et al. (2010). Characteristics of sedimentary facies in the fourth member of Shahejie Formation in wen 23 gas field. *Dongpu Depress. Fault-Block Oil Gas Field.* 17 (6), 726–728. CNKI:SUN:DKYT.0.2010-06-022.

Sun, S. (2007). Characteristics of transition structure in the Dongpu sag. *Petroleum Geol. Recovery Effic.* 23, 38–46. doi:10.3969/j.issn.1009-9603.2007.02.010

Sun, S., Peng, R., and Huang, S. (2006). Characteristics and origin of tranverse accommodation zones in the Dongpu subbasin, bohai gulf basin, and their role in regional sedimentation. *J. Geomechanics* 12 (1), 55–63. doi:10.3969/j.issn.1006-6616.2006.01.009

Tang, M., and Wang, H. (2008). Episodic characteristics of Fault and their effects on sedimentary and structural evolution during paleocene: a case study of Dongpu depression. *Mar. Geol. Quat. Geol.* 28 (3), 55–59.

Tchalenko, J. S. (1970). Similarities between shear zones of different magnitudes. *Geol. Soc. Am. Bull.* 81, 1625–1640. doi:10.1130/0016-7606(1970)81[1625:sbszod]2.0.co;2

Twiss and Moores (2007). *Structural geology*. second edition. W. H. Freeman and Company.

Wang, M., Sherwood, N., Li, Z., Lu, S., Wang, W., Huang, A., et al. (2005). Shale oil occurring between salt intervals in the Dongpu depression, bohai Bay Basin, China. *Int. J. Coal Geol.* 152, 100–112. doi:10.1016/j.coal.2015.07.004

Wang, R., Shen, P., and Zhao, L. (2011). Diagenesis of deep sandstone reservoirs and a quantitative model of porosity evolution: taking the third member of Shahejie Formation in the Wendong Oilfield, Dongpu Sag, as an example. *Petroleum Explor. Dev.* 38 (5), 552–559. (in Chinese with English abstract). doi:10.1016/S1876-3804(11)60055-4

Wang, R., Shi, W., Xie, X., Tang, D., Manger, W., Busbey, A. B., et al. (2018). Boundary fault linkage and its effect on upper jurassic to lower cretaceous sedimentation in the gudian half-graben, songliao basin, northeastern China. *Mar. Petroleum Geol.* 98, 33–49. doi:10.1016/j.marpetgeo.2018.08.007

Wang, T. (1997). *Hydrocarbon reservoir geology of rifting basins in eastern China*. Beijing, China: Petroleum Industry Press, 196.

Xu, H., Wang, X., Yan, D., and Qiu, L. (2018). Subsidence transition during the post-rift stage of the Dongpu Sag, Bohai Bay Basin, NE China: a new geodynamic model. *J. Asian Earth Sci.* 158, 186–199. doi:10.1016/j.jseaes.2018.03.001

Xu, Y., Li, Y., Pang, J., and He, B. (2009). On the timing and duration of the destruction of the north China craton. *Chin. Sci. Bull.* 54 (19), 3379–3396. doi:10.1007/s11434-009-0346-5

Yang, Q., Qi, J., Chen, X., et al. (2006). Disruibution of original stratigraphic thickness of each member in the Paleogene and its tectonopaleogeographic implication in Dongpu Sag, Henan Province. *J. Palaeogeogr.* 8, 407–413.

Yin, A. (2010). Cenozoic tectonic evolution of Asia: A preliminary synthesis. *Tectonophysics.* 488 (1–4), 293–325. doi:10.1016/j.tecto.2009.06.002

Young, M. J., Gawthorpe, R. L., and Hardy, S. (2001). Growth and linkage of a segmented normal fault zone: the late Jurassic Murchison–Statfjord North fault, northern North Sea. *J. Struct. Geol.* 23, 1933–1952. doi:10.1016/S0191-8141(01)00038-4

Yu, F., and Koyi, H. (2016). Cenozoic tectonic model of the bohai Bay Basin in China. *Geol. Mag.* 153 (5-6), 866–886. doi:10.1017/S0016756816000492

Zeng, L., Su, H., Tang, X., Peng, Y., and Gong, L. (2013). Fractured tight sandstone oil and gas reservoirs: a new play type in the Dongpu depression, Bohai Bay Basin, China. *AAPG Bull.* 97 (3), 363–377. doi:10.1306/09121212057

Zhai, G. M. (1993). *Petroleum geology of China (Vol.6):Shengli oil field (in Chinese)*. Beijing: Petroleum Industry Press.

Zhang, L., Zhang, S., Chen, Z., Zhang, C., and Hong, Z. (2004). The generation of immature oils in the lacustrine Jiyang mega-depression, Bohai Bay Basin, China. *J. Petroleum Geol.* 27 (4), 389–402. doi:10.1111/j.1747-5457.2004.tb00065.x

Zuo, H., Ye, B., Wu, W., Zhang, Y. x., Ma, W. x., Tang, S. l., et al. (2017). Present temperature field and cenozoic thermal history in the Dongpu depression, bohai Bay Basin, north China. *Mar. Petroleum Geol.* 88, 696–711. doi:10.1016/j.marpetgeo.2017.08.037